



Analysis of Temperature and Residual Stress Distribution in CO₂ Laser Welded Aluminum 6061 Plates Using FEM

Sanaa Numan Mohammed

Department of Manufacturing Operations/ Al-Khwarizmi College of Engineering/ University of Baghdad

(Received 22 February 2011; accepted 19 Jun 2011)

Abstract

This paper develops a nonlinear transient three-dimensional heat transfer finite element model and a rate independent three-dimensional deformation model, developed for the CO₂ laser welding simulations in Al-6061-T6 alloy. Simulations are performed using an indirect coupled thermal-structural method for the process of welding. Temperature-dependent thermal properties of Al-6061-T6, effect of latent heat of fusion, and the convective and radiative boundary conditions are included in the model. The heat input to the model is assumed to be a Gaussian heat source. The finite element code ANSYS12, along with a few FORTRAN subroutines, are employed to obtain the numerical results. The benefit of the proposed methodology is that it offers the capability of optimizing laser welding process, and also provides a reliable estimation of the developed temperatures, as well as the thermal stress (residual stress) and strain fields reducing the experimental effort.

Keywords: Laser welding; aluminum alloys finite element analysis.

1. Introduction

A successful lightweight construction is the result of an optimized combination of material selection, design and manufacturing. When the lightweight components are made from aluminum alloys, welding is one of the most widespread joining technologies available. In order to avoid costly trial-and error experiments and to improve the in-service quality of assemblies, numerical simulation of welding can be a powerful tool. Laser welding could be used in place of many different standard processes, such as resistance (spot or seam), submerged arc, RF induction, high-frequency resistance, ultrasonic and electron-beam. While each of these techniques has established an independent niche in the manufacturing world, the versatile laser welding approach will operate efficiently and economically in many different applications. Its versatility will even permit the welding system to be used for other machining functions, such as cutting, drilling, scribing, sealing and serializing. Laser beam welding has been identified as a promising method for joining aluminum in body

applications such as tailored blanks. Due to rapid heating and cooling, welding process produces inevitably large residual stresses in the engineering structures, which often approach the yield strength of the material. For the key components such as the welded joints in nuclear power plants, design and structural integrity assessments require an account of residual stresses. Therefore, measuring and predicting welding residual stresses are very important. Many of the advantages and limitations of laser welding, compared to other welding processes, depend on focused beam properties. The high power density permits welding based on the keyhole principle, and the reduced energy transfer to the material produces a very narrow heat affected zone (HAZ) with low residual stress and small distortions [1].

The aim of the present work is the employment of finite element (FE) method to assess thermal and mechanical fields in terms of temperature, stress and strain distributions in laser welded joints made of Al-6061-T6 alloy. The understanding of the heat-process of welding is important for the analysis of welding structure

mechanical and microstructure and controlling of welding quality [2]. Therefore, numerical simulation of the welding process has been a major topic in welding research for several years. The results of simulations can be used to explain the physical essence of some complex phenomena in welding process explicitly and also can be used as the basis for optimizing the welding parameters. A number of analytical and numerical models of welding processes have been used to evaluate temperature and stress distribution during and after the welding process, and predict the residual stresses and final distortions of structural components. These include analytical models [3-6], two dimensional finite element models [7, 8] and three dimensional finite element models of laser [9-12].

In the present investigation, a three dimensional finite element model for the laser welding simulation was developed. It considers a Gaussian distribution of heat flux using a moving heat source. A nonlinear thermo-mechanical analysis was performed using temperature dependent material properties.

2. Finite Element Analysis

In laser welding process the focal spot is targeted on the workpiece surface which will be welded. At the surface the large concentration of light energy is converted into thermal energy. The surface of the workpiece starts melting and progresses through it by surface conductance. For welding, a very narrow zone under the laser beam is suddenly heated, vaporized and locally fused. After welding and cooling the melted material, the assembly of the welded pieces is achieved. On the exposed area a keyhole is shaped. The elevated temperature gradients present in this area during both the heated and the cooling along with the sharp decrease of mechanical properties during heating, yield to nonhomogeneous permanent strains and residual stresses after the process.

A three dimensional transient, isotropic solid with moving heat source finite element model was developed to simulate the laser welding process using the commercial code ANSYS12. The finite element model is shown in Fig. 1. The whole length of the plate is 200mm, the width is 100mm and the thickness is 4 mm. For the solution, a thermo-elasto-plastic analysis was performed using the enhanced finite element with user FORTRAN subroutine. The solution was generated in two basic steps. First a transient heat transfer analysis was performed and the resulting

temperature field was used on the second step as an input to the mechanical analysis. An appropriate time-stepping scheme was used for each analysis to achieve fast convergence of the solution and reasonable accuracy.

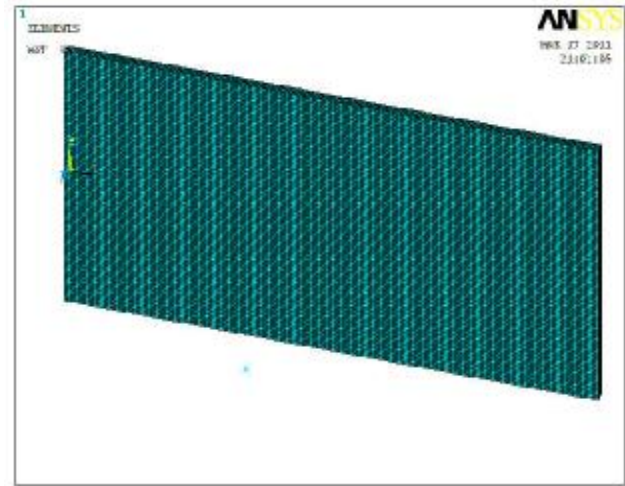


Fig.1. Three-Dimensional Finite Element Model.

Temperatures induced in the plate by irradiation can be calculated by the nonlinear transient thermal finite element equation (Eq. 1). As can be seen in the equation, the temperature-dependent material properties of the plate have to be involved for the nonlinear problem, and the time-dependent heat loads are required for the transient problem.

$$\left\{ k(T) \left(\frac{\partial^2 T}{\partial x^2} \right) + \left(\frac{\partial^2 T}{\partial y^2} \right) + \left(\frac{\partial^2 T}{\partial z^2} \right) \right\} + \dot{Q} = \rho(T) c_p(T) \left(\frac{\partial T}{\partial t} \right) \quad \dots(1)$$

Where x, y, z are the Cartesian coordinate, \dot{Q} (the internal heat generation), ρ (the density), k (the thermal conductivity) and C_p (the specific heat) are the functions of temperature T .

Three types of solid elements are commonly used for a three-dimensional model – brick, wedge, and tetrahedron. It is a primary condition to use the appropriate elements for finite element models to obtain the most accurate solution through the finite element analysis. In the present thermal analysis, the sheet metal is meshed using a brick element (called SOLID70) because the element is more accurate and more computationally efficient than a comparable tetrahedron one. Figure 2a shows the geometry, node locations, and the coordinate system of SOLID70, which has eight nodes with a single degree of freedom, temperature, at each node.

Heat fluxes and convections can be an input as surface loads at the element faces as shown by the circled numbers on the element geometry. The surface loads are defined with the nodes or elements. An advantage of the use of the element is that this element can be replaced by an equivalent structural element for structural analysis. For the consideration of the radiation effect on the plate surface, a three dimensional thermal surface effect element (SURF152) is used overlaying it onto the faces of the base elements made by SOLID70. Figure 2b shows the geometry, node locations, and the coordinate system of the element, which is defined by four to nine nodes and the material properties (e.g., emissivity). An extra node has to be generated to reflect the radiation effect, which is positioned away from the base element. For mechanical analysis, a structural element defined by eight

nodes (i.e., SOLID45) is used for three dimensional modeling of the plate. Each node of the element has three degrees of freedom: translations in the nodal x, y, and z directions. The element supports analysis of plasticity, large deflection, large strain, stress stiffening, creep and swelling. For the structural analysis, the heat transfer model containing the equivalent thermal element SOLID70 can be replaced by this element, and temperatures obtained from the thermal step can be applied as element body loads at the nodes. The geometry, node locations, and the coordinate system of this element are equal to the SOLID70 (See Figure 2 a). Figure (1) shows the meshes generated for the present simulation. The meshes are composed of a total number of 80,000 solid elements and 20,000 surface elements.

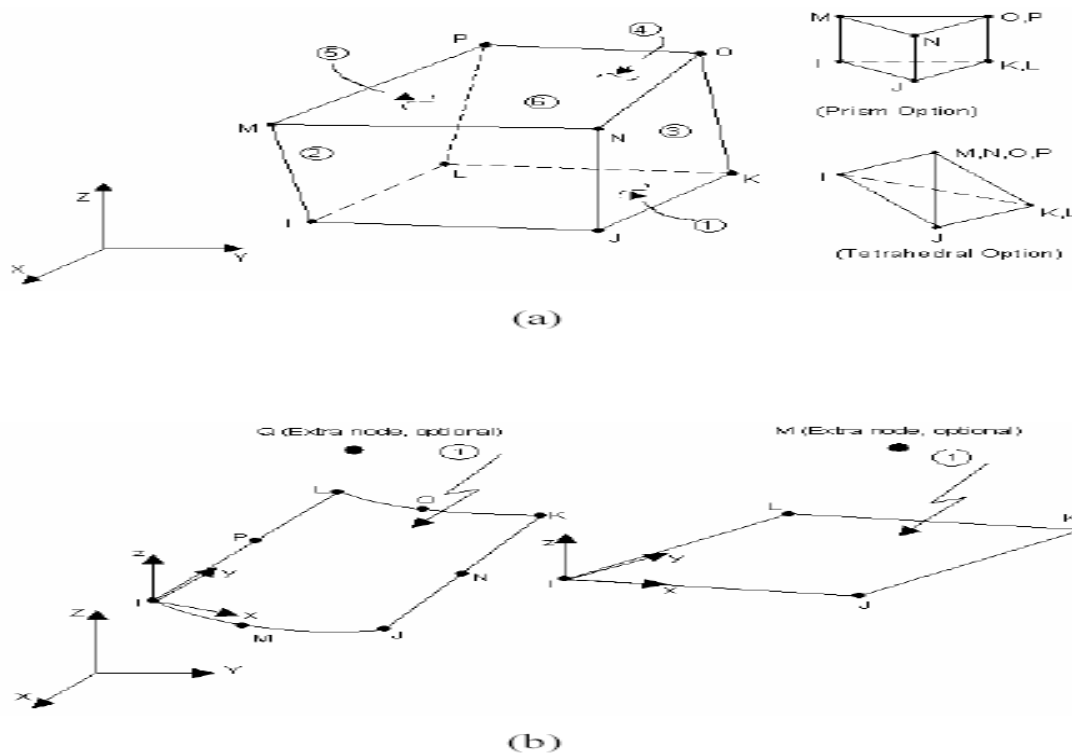


Fig.2. Geometries of: (a) The Three-Dimensional Thermal Solid Element, SOLID70; and (b) The Thermal Surface Effect Element, SURF152.

3. Material Properties

As can be seen in Eq.(1), temperature response in a material involved in high heat fluxes is determined by the thermal material properties of thermal conductivity, specific heat, and density, which are dependent on temperatures. The accurate calculation of temperatures is critical in

laser welding because bending variables of stress and strain are dependent on temperatures. Therefore, temperature dependent thermal properties of Al-6061-T6 plate are used in the finite element model. The thermal material properties of Al 6061-T6 are presented in Fig. 3, after ref. [13], while temperature dependent material mechanical properties Young's Modulus,

Poisson's Ration, density and thermal expansion coefficient are presented in Fig. 4.

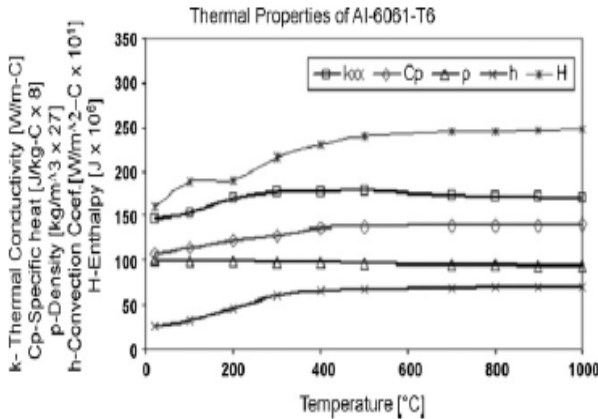


Fig.3 Thermal Properties for Al alloy 6061-T6 (After Ref. [13]).

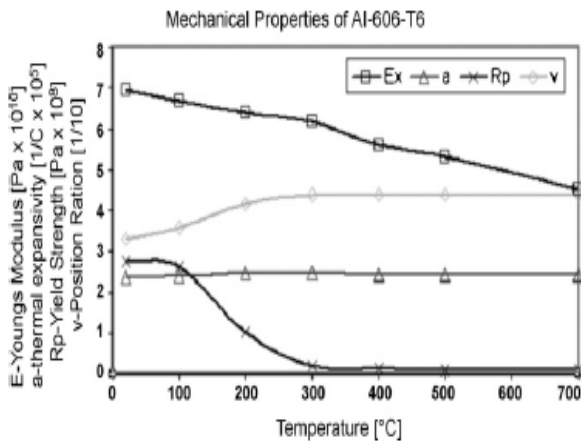


Fig.4. Mechanical Properties for Al Alloy 6061-T6.

4. Thermal Analysis

4.1. Heat Flux Input

The heat intensity on the plate surface by laser beam is modeled as an idealized Gaussian distribution, and the heat flux is described as follows:

$$q(r) = \frac{2\eta P}{\pi R^2} \exp\left(-\frac{2r^2}{R^2}\right) \quad \dots(2)$$

Where:

- $q(r)$ = the intensity of the incident heat flux at the material surface
- η = heat transfer efficiency
- P = beam power
- R = beam diameter
- r = distance from the center of the laser beam

The mean thermal flux density $\bar{q}(r)$, within the area of the laser beam is calculated from Eq. (2) as follows [14]:

$$\begin{aligned} \bar{q}(r) &= \frac{1}{\pi R^2} \int_0^R q(r) \cdot (2\pi r) dr \\ &= \frac{2\pi}{\pi R^2} \int_0^R \frac{2\eta P}{\pi R^2} \exp\left(-\frac{2r^2}{R^2}\right) r dr \\ &= \frac{0.865\eta P}{\pi R^2} \quad \dots(3) \end{aligned}$$

In the present simulation, the heat flux, $\bar{q}(r)$ obtained from Eq. (3) is used as a surface load, and the load is imposed on the selected set of element faces of the plate surface. The movement of the laser beam is realized by adopting the local coordinate system to apply heat loads as a step. As shown in Figure (5), the local coordinates are generated along the heating line as defined steps first; then at each step, the center of the laser beam is located at the origin of the local coordinate and the heat load is applied on the elements placed inside the laser beam (illustrated line circle). In order to ensure convergence, the heat loads are imposed by small increments using *DO loop command.

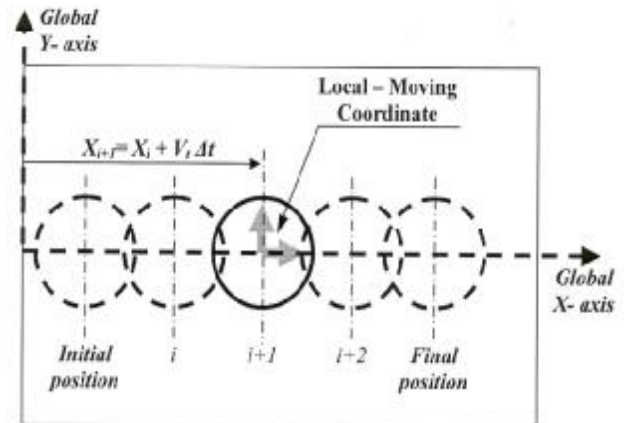


Fig.5. Local Coordinates and Laser Beams Related to the Coordinates.

The heating time, t_s , at each step is described as follows:

$$t_s = \frac{l_p}{v_s} \cdot \frac{1}{n_e} \quad \dots(4)$$

Where:

- l_p = length of plate, v_s = speed of laser beam, n_e = number of elements along the heating line.

The numerical values for heat source parameters used in this paper are shown in Table1.

Table 1,
Simulation Conditions of the Laser Welding Process.

Laser power (W)	Scanning speed (mm/s)	Beam Diameter (mm)	Number of irradiation
1500	10	12	1

4.2. Boundary Conditions

Three boundary conditions associated with equation (1) are shown in figure (6).

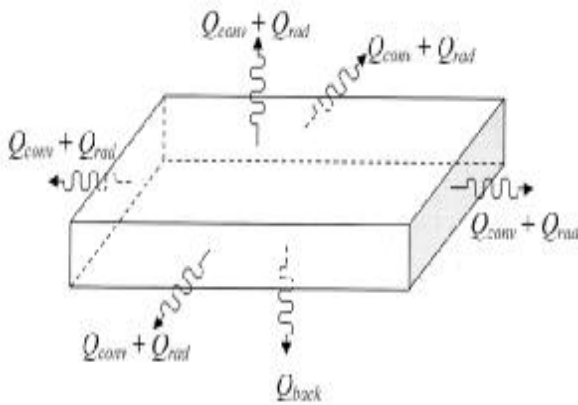


Fig.6. Thermal Boundary Conditions.

The boundary conditions used include:

- Adiabatic condition is considered on the laser path due to symmetry.
- Heat losses from the plate surfaces to the surroundings take place by means of natural convection and radiation effects.

For the radiant heat loss, q_r ,

$$q_r = \sigma \epsilon_r (T_r^4 - T_\infty^4) \quad \dots(4)$$

Where:

σ = the Stefan-Boltzmann constant ($\sigma=5.67 \times 10^{-8} \text{ W/m}^2 \cdot \text{K}^0$)

ϵ_r = the emissivity of radiating surface ($\epsilon_r=0.5$)

T_r = the absolute temperature of radiating surface

T_∞ = the absolute temperature of surrounding ($T_\infty=298 \text{ K}^0$)

For the convective heat loss, q_c ,

$$q_c = h_f (T_s - T_\infty) \quad \dots(5)$$

Where:

h_f = the convection coefficient ($h=30 \text{ W/m}^2 \cdot \text{K}^0$)

T_s = the temperature at the plate surfaces

5. Mechanical Analysis

A non-linear mechanical analysis is executed just after each thermal analysis step, in order to calculate stress and strain distributions of the structure. The results of the thermal analysis step (transient temperature distribution) serve as loading to the corresponding mechanical analysis step. The introduced temperature dependent material mechanical properties Young's Modulus, Poisson's Ration, density and thermal expansion coefficient are presented in Fig. 4. In the mechanical simulation, the elastic behavior is modeled using the isotropic Hooke's rule with temperature-dependent Young's modulus. The thermal strain is considered using thermal expansion coefficient. For the plastic behavior, a rate-independent plastic model is employed. The yield criterion is the Von Mises yield surface. In the present numerical model, the strain hardening is taken into account using the isotropic hardening law. The non-linear mechanical analysis problem is described by the following general FE equation:

$$[K(T)]\{u(t)\} + \{F(t)\} + \{F^{th}(t)\} = 0 \quad \dots(6)$$

where $K(T)$ is the temperature-dependent stiffness matrix; $F(t)$ the external load vector; $F^{th}(t)$ the temperature load vector; $\{u(t)\}$ is the displacement vector. The Newton-Raphson algorithm is utilized for solving the non-linear equation system and the Newmark integration scheme is applied for the numerical integration in the time domain. The mechanical boundary conditions are constrained only for preventing rigid body motion with considering symmetry. The simulations are conducted on a personal computer with a 2.1GHz CPU and a 4.0GB memory. The total computational time used is 28 h or so.

6. Simulation Results

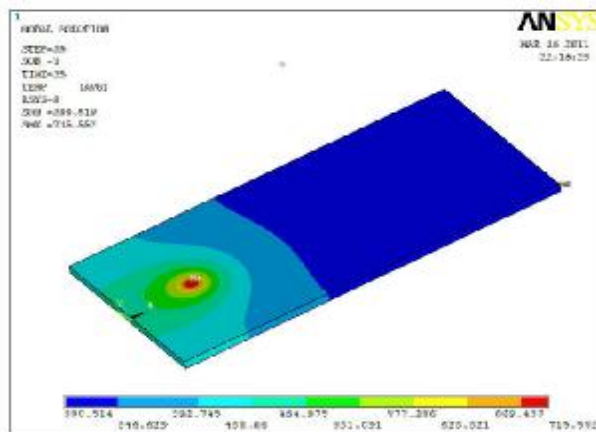
6.1. Temperature and Residual Stresses Field Induced by Laser Beam Welding

Using the geometry, the mesh and the heat flux distribution model described above and the geometrical parameters of the welded pool, the thermal analysis was first conducted. Figures 7(a)-(d) show the temperature distribution on the welding parts at four different times during the process. The figures show clearly the large temperature gradients at the area close to the laser beam and also indicate the cooling of the workpieces away from the heat source. Figure 7a shows temperature distribution on the surface of

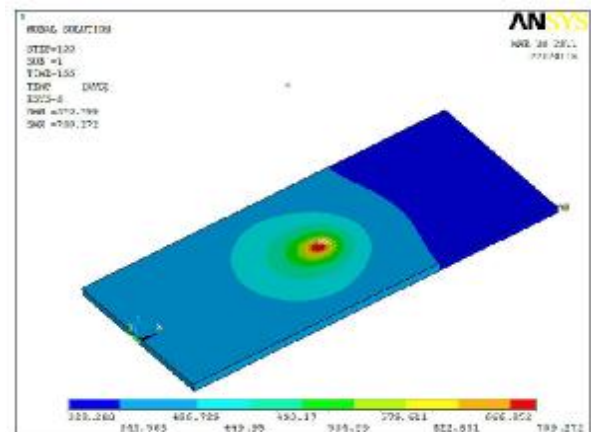
the welded plate at time $t= 35$ Sec (i.e. at the beginning of the welding process). Figure 7b shows temperature distribution on the surface of the welded plate at time $t= 100$ Sec (i.e. when the laser beam is passing the center of the plate) while figure 7c indicate the temperature distribution at the last step of heating process. Figure 7d shows the situation (temperature distribution) after cooling. Figure 8 is captured from the left side view on the X-Z plane crossing the centre of the plate. It is noted that the maximum temperature occurs in the rear of the centre of the beam during heating, and the temperature gradient is steeper in the front of the centre of the beam than that in the rear. The keyhole shape from the FE analysis is shown in Figure 8, this shape gives good approximate shape for the weld pool measured by many experimental studies. Figure 9a shows The temperature history at a node in the welding zone of the plate. The temperature rises rapidly and reaches a maximum of nearly 861 °K and then subsequently drops smoothly at the same rate when the laser beam moves away from the welding point, indicating that the steep temperature gradient collapses rapidly. Figure 9b

shows the temperature distribution across a perpendicular path to the welding line; the figure indicates that the temperature is maximum in the center of the welding zone and decreases gradually at the ends.

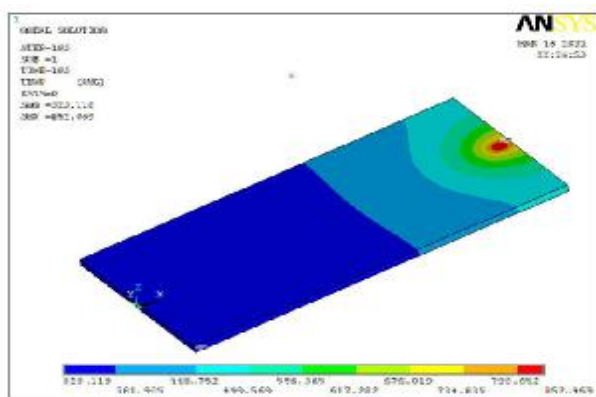
To evaluate the residual stress distribution, the heat transfer analysis was performed first in order to find nodal temperatures as a function of time, and then in the second part of the analysis, a non-linear mechanical analysis was carried using the temperature distributions which were obtained from the heat transfer model. Temperature fields affect mechanical fields through thermal expansion and temperature dependent material properties. Thermal expansion or contraction due to transient application of temperature gradients is usually the dominant concern in thermal stress analysis. The non-linear mechanical properties were used as shown in figure (4) and the yield criterion used is the Von Mises yield surface. The mechanical boundary conditions are constrained so that the two edges of the plate parallel to welding line are fixed to prevent rigid body motion.



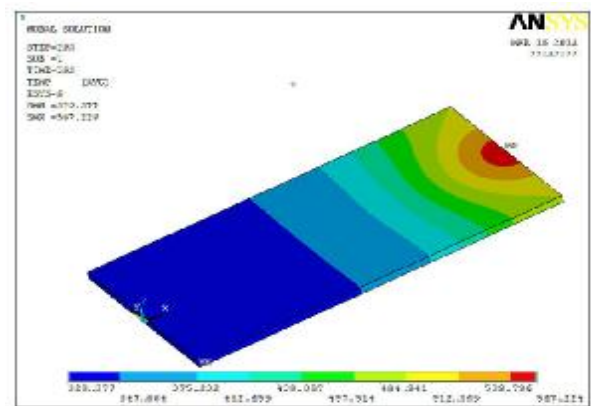
-a-



-b-



-c-



-d-

Fig.7. Temperature Distributions at: (a) 35 sec; (b)100 sec; (c) 193 sec; and(d) 203 sec.

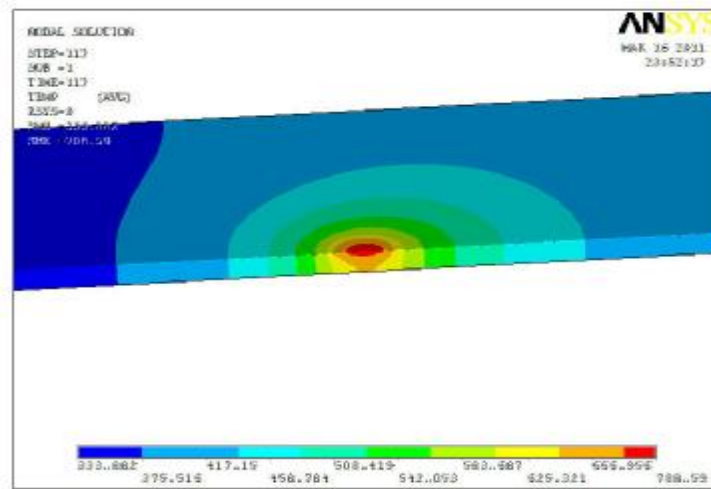


Fig.8. Keyhole Shape and Temperature Distributions Through the Thickness Direction at 117 Sec.

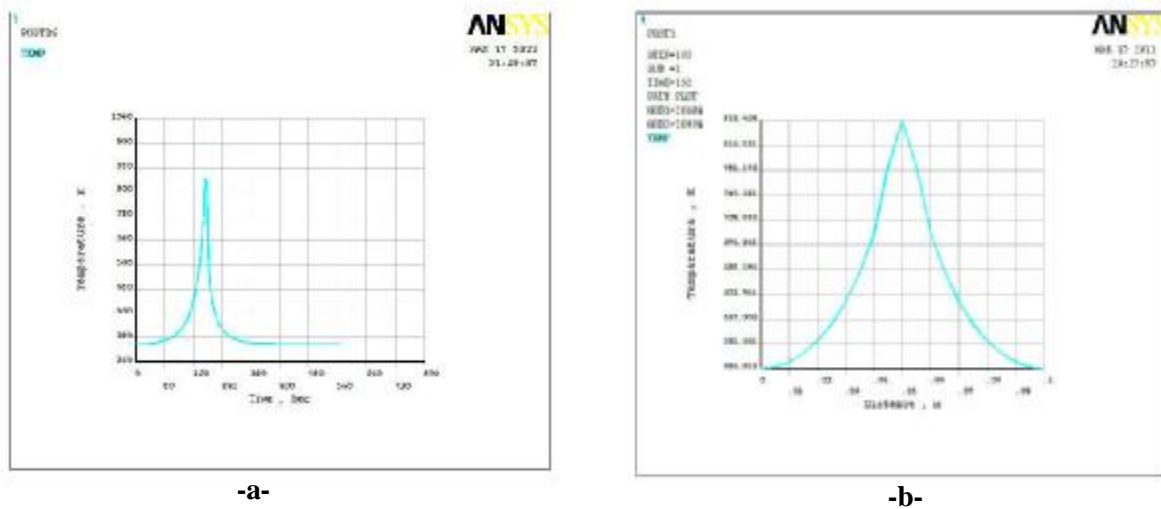


Fig.9. (a) Temperature History for a Node in the Weld Zone. (b) Temperature Distribution Across a Path Perpendicular to the Welding Line.

Longitudinal and transverse stresses at different times are shown in Figures (10&11); the positive stress values representing the red region indicate the tensile stresses, and the negative stress values representing the blue region indicate the compressive stresses. Figure (10) shows the stress distributions on the plate surfaces at four different stages of the process – when the heating is at the early stage (t = 35 sec) (a), when the laser beam is passing the center of the plate (t =100 sec) (b), when the operation is finished (t = 193 sec) (c) and , when the plate is cooled (t = 519 sec) (d). It is noticed from Figure (10) (a) that when the heating begins, high compressive stresses of a maximum of 131 MPa arise in the heated surface and its neighboring zone due to thermal expansion by high temperatures. Tensile

stresses are produced in the region in front of the laser beam to counteract the thermal expansion constraining material in the surrounding. During the cool down phase of the heated zone, as shown in Figure (10), the compressive stresses change to tensile stresses (a maximum of 121 MPa) due to the contraction of the heated zone. After the operation, the tensile stresses remain at the surface along the centerline of the plate.

The shape of the residual stress (longitudinal) is shown in figure (12a). The figure indicates that after cooling the stresses are tensile in the center of the plate while they are compressive in the edges; the reason for this behavior can be found in the fact that recrystallization reduces the extent of residual stresses, that is higher at the interface between the mechanical stressed zone and the heat

affected zone. Figure (12b) shows normal stresses orthogonal to the direction of the weld known as

transverse residual stresses.

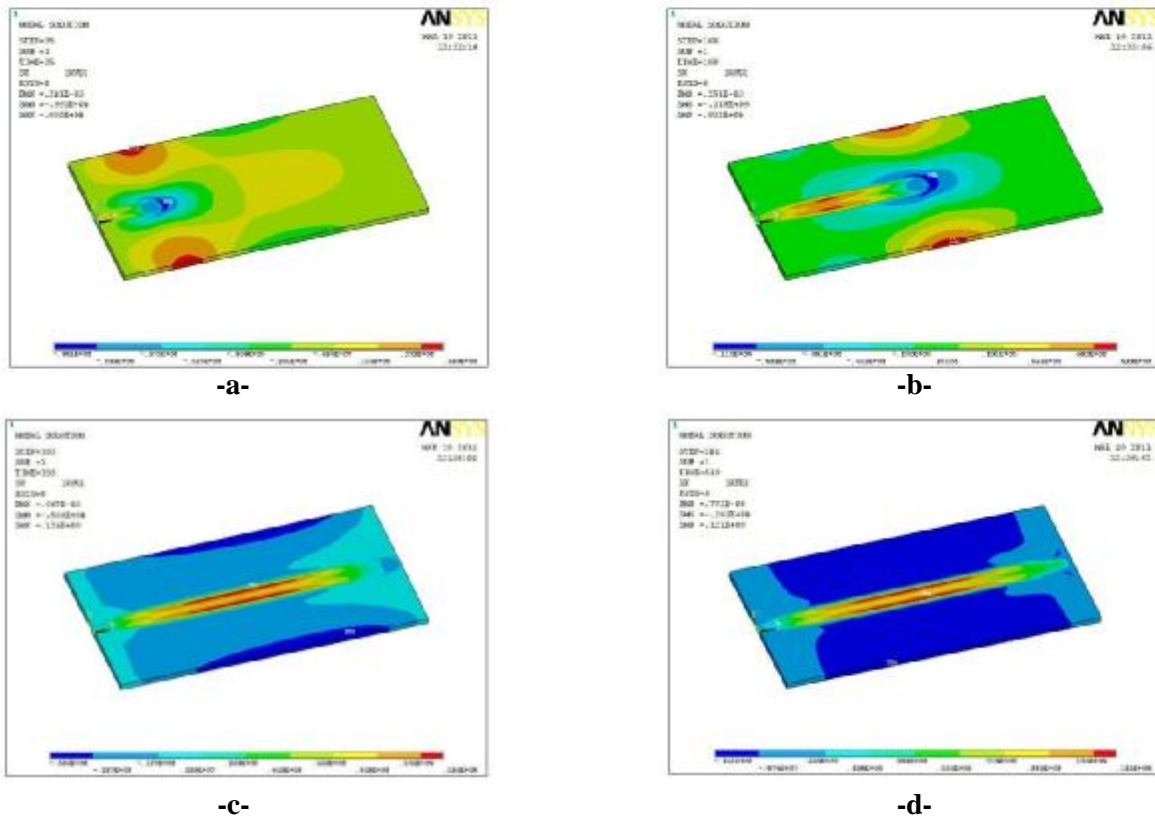


Fig.10. Stress Distribution in X-Direction at Different Times a-35 sec, b-100 sec, c-193 sec and d-519 sec.

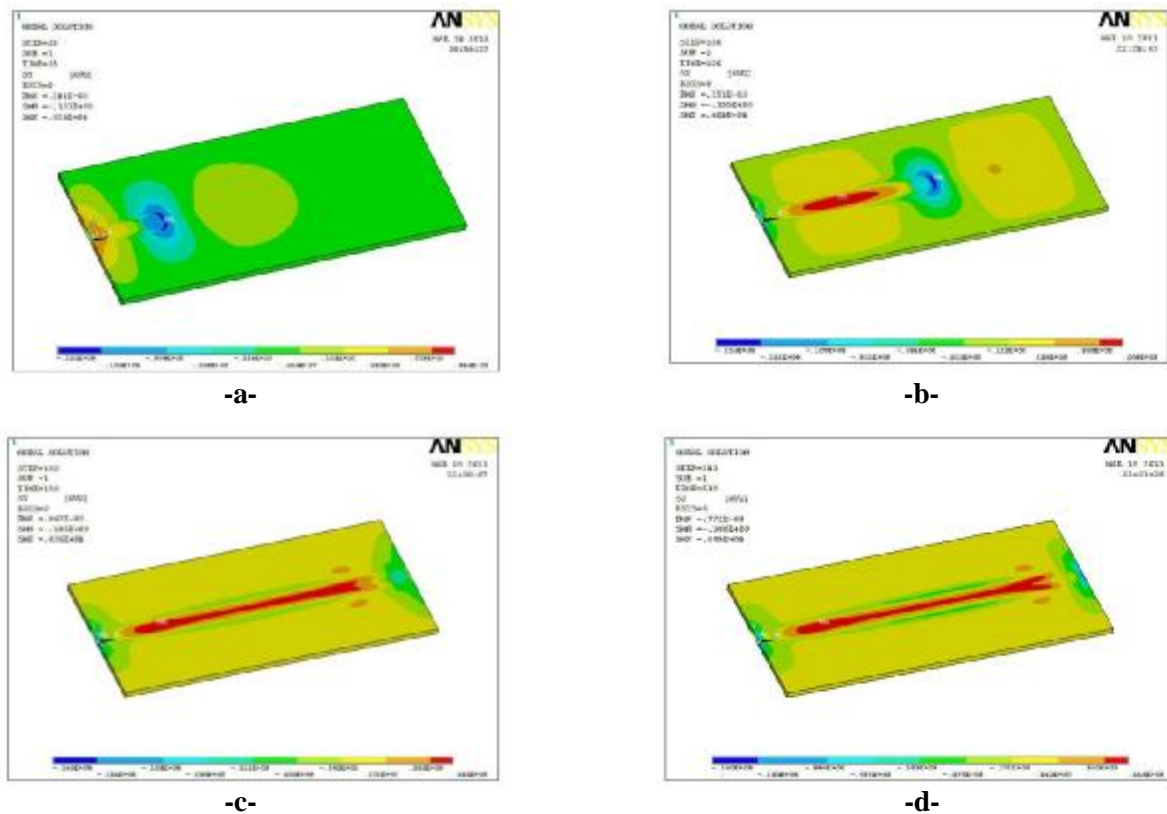


Fig.11. Stress Distribution in Y-Direction at Different Times a-35 sec, b-100 sec, c-193 sec and d-519 sec.

- [12] D. H. Kang, K. J. Son, Y.S. Yang. Analysis of laser weldment distortion in the EDFA LD pump packaging, finite element analysis Des., vol 37, 2001, pp. 749-760.
- [13] Soundararajan, V., Zekovic, S., Kovacevic, R., Thermo-mechanical model with adaptive boundary conditions for friction stir welding of Al 6061. Int. J. Mach. Tools Manuf. 45,2005 1577–1587.
- [14] Hu, Z., etal. Computer simulation and experimental investigation of sheet metal bending using laser beam scanning., international journal of machine tools and manufacture, 2001, 41(4), pp.589-607.

تحليل توزيع درجات الحرارة والاجهادات المتبقية في صفائح الألمنيوم 6061 الملحومة بالليزر باستخدام طريقة العناصر المحددة

سنة نعمان محمد

قسم هندسة عمليات التصنيع/كلية الهندسة الخوارزمي/جامعة بغداد

الخلاصة

في هذا البحث تم تطوير نموذج ثلاثي الأبعاد لاختي لنمذجة عملية الانتقال الحراري والتشوه الميكانيكي الحاصل في عملية اللحام بالليزر في سبائك الألمنيوم T6-6061. تم استخدام أسلوب المحاكاة الحراري والهيكلية المقترن اللامباشر في عملية اللحام. ولكون النموذج المقترح هو لاختي فقد استخدمت خواص حرارية وميكانيكية متغيرة مع درجة الحرارة مع الأخذ بنظر الاعتبار الظروف المحيطة بالعملية مثل الحمل الحراري والإشعاع. تم التحليل باستخدام برنامج ANSYS12 مع بعض البرامج الداعمة والتي كتبت بلغة FORTRAN. الفائدة المتوخاة من هذا البحث هو انه يمكن اعتماد المنهجية المقترحة في دراسة وتحليل عملية اللحام بالليزر وما يرافقها من تشوهات واجهادات حرارية وبالتالي الحصول على عملية لحام مثلى.